

High-speed label-free two-photon fluorescence microscopy of metabolic transients during neuronal activity

Cite as: Appl. Phys. Lett. **118**, 081104 (2021); doi: 10.1063/5.0031348

Submitted: 29 September 2020 · Accepted: 3 February 2021 ·

Published Online: 23 February 2021





View Online



Export Citation



CrossMark

Andrew J. Bower,^{1,2}  Carlos Renteria,^{1,3}  Joanne Li,^{1,3}  Marina Marjanovic,^{1,3,4} Ronit Barkalifa,¹ and Stephen A. Bopp^{1,2,3,4,a)} 

AFFILIATIONS

¹Beckman Institute for Advanced Science and Technology, University of Illinois at Urbana-Champaign, Urbana, Illinois 61801, USA

²Department of Electrical and Computer Engineering, University of Illinois at Urbana-Champaign, Urbana, Illinois 61801, USA

³Department of Bioengineering, University of Illinois at Urbana-Champaign, Urbana, Illinois 61801, USA

⁴Carle Illinois College of Medicine, University of Illinois at Urbana-Champaign, Urbana, Illinois 61801, USA

^{a)}Author to whom correspondence should be addressed: boppart@illinois.edu

ABSTRACT

The brain is an especially active metabolic system, requiring a large supply of energy following neuronal activation. However, direct observation of cellular metabolic dynamics associated with neuronal activation is challenging with currently available imaging tools. In this study, an optical imaging approach combining imaging of calcium transients and the metabolic co-enzyme nicotinamide adenine dinucleotide (phosphate) (NAD(P)H) is utilized to track the metabolic dynamics in hippocampal neuron cultures. Results show distinct cellular components for the NAD(P)H response following neuronal activity, where notable differences in the NAD(P)H dynamics between neurons and astrocytes can be directly observed. Additionally, tracking of these responses across a large field of view is demonstrated for metabolic profiling of neuronal activation. Observation of neuronal dynamics using these methods allows for closer examination of the complex metabolic machinery of the brain, and may lead to a better understanding of the cellular metabolism of neuronal activation.

Published under license by AIP Publishing. <https://doi.org/10.1063/5.0031348>

While the human brain represents approximately 2% of body weight, it represents 20% of the total oxygen consumption of the body.¹ Early investigations of this dynamic system through functional imaging studies based on positron emission tomography surprisingly revealed that neural activity led to increased rates of glucose consumption compared to rates of oxidative metabolism.² Similarly, many optical imaging investigations have observed strong reduced nicotinamide adenine dinucleotide (phosphate) (NAD(P)H) and flavin adenine dinucleotide autofluorescence transients following electrical stimulation in brain slices, first reported by Lipton in 1973.³ While neuronal metabolic dynamics at the organ scale have been well characterized, the cellular basis of these processes is still a matter of scientific debate.

At the heart of this debate is the *in vitro* observation that astrocytes will undergo aerobic glycolysis, converting glucose to lactate following glutamate uptake.⁴ Further supported by observations that lactate can serve as a primary substrate for neuronal oxidation,^{5,6} this led to the development of the astrocyte-neuron lactate shuttle (ANLS) model, which contends that astrocytes and neurons have distinct

metabolic phenotypes and that astrocytes specifically produce lactate to provide neurons with a secondary substrate for oxidative metabolism. While evidence has emerged both supporting^{7,8} and opposing^{9–12} this model, high-speed cellular-resolution optical microscopy has been an important tool to study this complex system.^{7,9} NAD(P)H transients, in particular, have been used extensively to study metabolic processes during neuronal activation.¹³ Kasischke *et al.* used high-resolution two-photon autofluorescence microscopy of brain slices to show that the “dip” and “overshoot” phases of the characteristic NAD(P)H biphasic response following stimulation have distinct regional origins corresponding to areas of neurons and astrocytes, respectively.⁷ These observations fit nicely into the ANLS model as the observed astrocytic glycolysis following the initial neuronal oxidative metabolism signal suggests a potential increase in lactate production to be shuttled to neurons as a secondary substrate for further oxidative metabolism. However, contradictory evidence has been presented recently suggesting that the neuronal response is glycolytic in nature, motivating the need for direct methods of assessing the cellular

metabolic dynamics following neuronal activation.⁹ Across these studies, the inability to directly observe metabolic dynamics at the cellular level has served to further fuel this debate.

These conflicting results highlight some of the challenges that must be overcome to further study this complex process. In particular, two-photon NAD(P)H-based imaging methods are highly sensitive to the NAD(P)H content of the cell and potentially to specific levels of protein binding, but are typically burdened by the poor signal-to-noise ratio (SNR) and slow acquisition rates relative to neuronal dynamics. Two-photon fluorescence lifetime imaging microscopy (2P-FLIM), when used to image NAD(P)H, provides added specificity in distinguishing the relative free and protein-bound proportions of the NAD(P)H fluorescence emission¹⁴ and has enabled the sensitive measurement of cellular metabolism useful in the study of cancer development,¹⁵ therapeutic efficacy,¹⁶ and cell death.^{17,18} NAD(P)H lifetime imaging has the additional benefit of being more robust to sample-induced effects such as optical absorption and scattering.¹⁵ Recent work incorporating 2P-FLIM to study brain metabolism in an *in vivo* rat model revealed a complex molecular environment of NAD(P)H, demonstrating the sensitivity of this imaging method.¹⁹ However, most studies based on state-of-the-art instrumentation report image integration times on the order of minutes for 2P-FLIM NAD(P)H imaging,²⁰ which is considerably slower than the NAD(P)H biphasic response. Here, we incorporate two-photon fluorescence (2PF) calcium imaging into an existing custom-built high-speed 2P-FLIM imaging platform to permit direct observation of rapid metabolic dynamics following neuronal activation at the cellular level.

All animal procedures were performed under protocols approved by the Institutional Animal Care and Use Committee (IACUC) at the University of Illinois at Urbana-Champaign. Mouse hippocampi were isolated from P2-P3 transgenic mice (C57BL/6J-Tg(Thy1-GCaMP6s) GP4.12Dkim/J, Jackson Labs) following decapitation and either used immediately for culturing or stored on ice in Hibernate-A (HA, BrainBits) at 4 °C for one day and used the following day for culture. Hippocampal tissue was rinsed twice with 10 ml of HA and subsequently agitated with an HA-Calcium/papain (0.5 ml/mg) mixture in DI water. Thereafter, the tissue was mechanically dissociated by withdrawal twice with a 20 G needle attached to a 20 ml syringe. This was repeated once more with a 22 G needle. The dissociated cells were then filtered using a 20 μ m filter and centrifuged at 2000 rpm for 6 min. The supernatant was then removed with vacuum, and the cells were suspended in 500 μ l of Dulbecco's Modified Eagle Medium (DMEM). Upon suspension, the cells were counted using a hemocytometer and plated onto glass-bottom 35 mm culture dishes (Mat-Tek) to a final density of 200 000 cells per dish plated in 40 μ l of DMEM. These cells were then placed in a cell culture incubator (5% CO₂, 37 °C) for an hour. Finally, 500 μ l of pre-incubated DMEM and 1 ml of NBActiv4 were added to the culture. These primary cultures contain a mix of neurons and glia and are well established as a model for investigating cellular level behavior of the active, living brain.²¹

In this study, a previously described custom-built high-speed 2P-FLIM platform²² was modified to allow both 2PF NAD(P)H and calcium imaging. Briefly, a tunable titanium:sapphire laser (Spectra-Physics Mai Tai HP) was used as the excitation source and centered at 750 nm for the 2P-FLIM imaging system and 920 nm for calcium imaging using GCaMP6s, an intracellular label for tracking calcium dynamics.²³ The beam was scanned across the focal plane of the

microscope using an 8 kHz resonant scanner (EOPC SC-30) for the fast axis and a galvanometer scanning mirror (Cambridge Technology) for the slow axis. The emitted fluorescence was collected in the epi-direction through a 1.05 NA water immersion objective (Olympus XLPLN-25X-WMP2—1.05 NA; 25 \times magnification) and detected using a compact analog photomultiplier tube (PMT) (Hamamatsu H10721-20). The signal photocurrent generated by the PMT was amplified by a high gain transimpedance amplifier (Hamamatsu C5594) and sampled using a high-speed digitizer (AlazarTech ATS 9360) at 1.6 gigasamples per second. To further study dynamic NAD(P)H transients and specifically to track neuronal firing dynamics, the high-speed 2P-FLIM system was modified to enable 2PF imaging at an excitation wavelength of 920 nm in order to image GCaMP6s-labeled mouse hippocampal neuron cultures. This enables spatial correlation of the obtained metabolic signatures with neuronal calcium signals.

Figure 1 shows an example dataset from GCaMP6s-labeled hippocampal neuron cultures combining 2PF and 2P-FLIM imaging of NAD(P)H with calcium imaging of spontaneous neuronal activity. Imaging was performed by first collecting data at an excitation of 920 nm in order to excite GCaMP6s fluorescence [Fig. 1(a)], which was used to guide imaging toward a region with spontaneously firing neurons, seen as bright cells with a dynamic GCaMP6s fluorescence signal. Following this, the excitation wavelength was tuned to 750 nm for 2PF and 2P-FLIM imaging of NAD(P)H [Figs. 1(b) and 1(d), respectively]. 2P-FLIM images were acquired here with temporal integration over one second (20 individual frames acquired at 20 frames per second) with no spatial binning or filtering applied. This approach permits specific identification of neurons, labeled by GCaMP6s, in NAD(P)H 2PF and 2P-FLIM images, as seen by the overlay of GCaMP6s (green) and NAD(P)H (magenta) 2PF images in Fig. 1(c). Direct imaging and validation of neuronal dynamics have been challenging in previous studies due to high tissue density, the large NAD(P)H fluorescence signal from the background neuropil, and the relatively low NAD(P)H fluorescence that could be observed from neurons [Figs. 1(a)–1(d), white arrows and white box]. Here, the neuronal structure can be directly imaged and validated despite the dim NAD(P)H fluorescence observed from these cells. These results are consistent with previous reports of 2PF imaging in brain slices, where an increased NAD(P)H fluorescence emission is observed from surrounding glial cells, established to be astrocytes, while a dim NAD(P)H signal is seen in the surrounding neuropil.

Interestingly, 2P-FLIM [Figs. 1(d) and 1(e)] exhibits a relatively uniform lifetime across both neurons and astrocytes. These observations could be influenced by a few important factors. First, the NAD(P)H signature from neurons is quite weak, which may lead to the acquisition of a lower SNR fluorescence decay curve. Additionally, the axial resolution of 2P-FLIM is considerably lower than the transverse resolution,²⁴ and it is possible that background fluorescence from other cells may be contributing to the observed lifetime. Finally, it is possible that there is some effect of GCaMP6s on the registered fluorescence lifetime, either through the direct measurement of residual GCaMP6s fluorescence or through indirect interactions between GCaMP6s with NAD(P)H.

Next, longitudinal video-rate imaging was performed to investigate the fluorescence dynamics of these cells following a procedure similar to our previous study.²² Longitudinal 2PF and 2P-FLIM

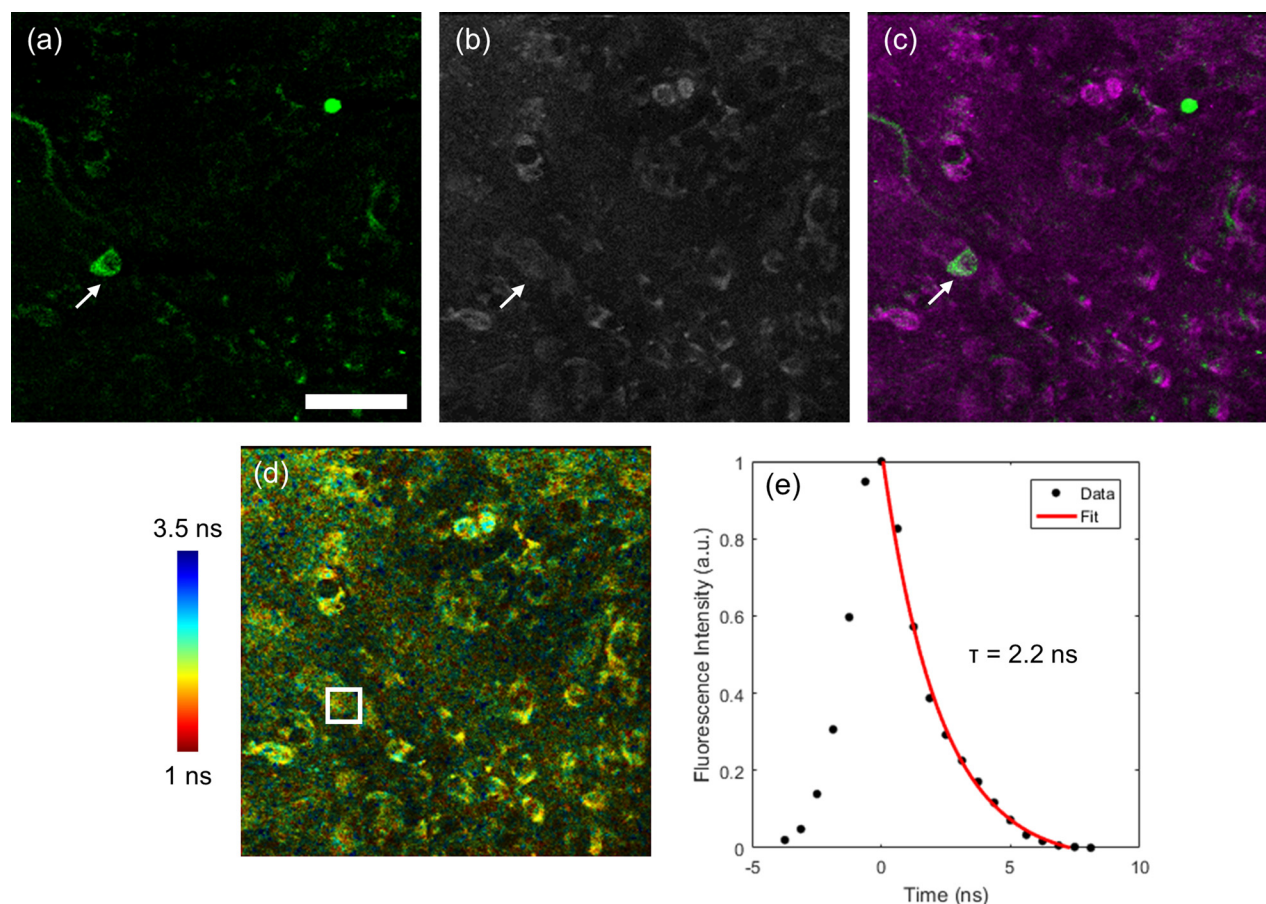


FIG. 1. 2PF and 2P-FLIM imaging of spontaneous activity in dissociated GCaMP6s mouse hippocampal neuron cultures. Images of (a) 2PF GCaMP6s, (b) 2PF NAD(P)H intensity, and (d) 2P-FLIM NAD(P)H allow combined detection of neuronal activity with metabolic imaging. (c) Overlay of the 2PF NAD(P)H intensity (magenta) and GCaMP6s (green) channels provides specific identification of NADH neuronal features (white arrows and white box), such as the weaker, more diffuse fluorescence emission from this region compared to neighboring glial cells. (e) 2P-FLIM decay curve constructed by summation of the fluorescence decay signal over the 20×20 pixel region of interest (ROI) denoted by the white box in (d), corresponding to a neuron. The scale bar represents $50 \mu\text{m}$.

images were acquired over a total recording time of 2 min. During longitudinal imaging, fresh culture media supplemented with glutamate (L-glutamic acid, Sigma) was introduced into the culture dish to a final concentration of $100 \mu\text{M}$ to stimulate neuronal activity. For longitudinal videos, temporal integration of images over 5 s (100 individual frames acquired at 20 frames per second) was performed. For display and image analysis, a Gaussian spatial filter ($\sigma = 1, 5 \times 5$ pixel kernel size) was further applied to the datasets to improve the SNR of the fluorescence decay curves at each pixel. 2PF results obtained from NAD(P)H and GCaMP6s imaging are shown in Fig. 2 (Multimedia view). As before, GCaMP6s imaging was first utilized to find a region exhibiting some amount of spontaneous activity observed through fluorescence intensity dynamics associated with intracellular calcium transients [Fig. 2(a)]. From images acquired before [Fig. 2(b)] and 2 min following glutamate addition [Fig. 2(c)], a sharp decrease in NAD(P)H fluorescence emission can be observed from a subpopulation of cells within the field of view (FOV) [Fig. 2(b) and 2(c), red arrows]. In surrounding cells, NAD(P)H fluorescence dynamics were more subtle, showing a small

increase in NAD(P)H fluorescence intensity over the acquisition window [Figs. 2(b) and 2(c), blue arrows].

To assess the spatial confinement of these transient NAD(P)H fluorescence dynamics, a difference image was constructed by subtracting the image of Figs. 2(c) from Fig. 2(b) and is shown in Fig. 2(d). This image shows a strong spatial confinement of this NAD(P)H decrease within cells that are co-localized with the positions of several active neurons identified through GCaMP6s imaging [Fig. 2(a)]. Longitudinal plots of the summed NAD(P)H fluorescence across each image of the video acquisition [Fig. 2(e)] demonstrate a distinct “dip” phase associated within a subset of cells consistent with the patterns seen in GCaMP6s-labeled neurons and an “overshoot” phase in many of the remaining cells consistent with previous reports for astrocytes within the FOV. Cells were segmented using CellProfiler²⁵ software and separated into two groups based on these metabolic dynamics. Single cell longitudinal traces of NAD(P)H dynamics shown in Fig. 2(f) (neurons) and Fig. 2(g) (astrocytes) provide direct evidence of distinct NAD(P)H dynamics among astrocytes

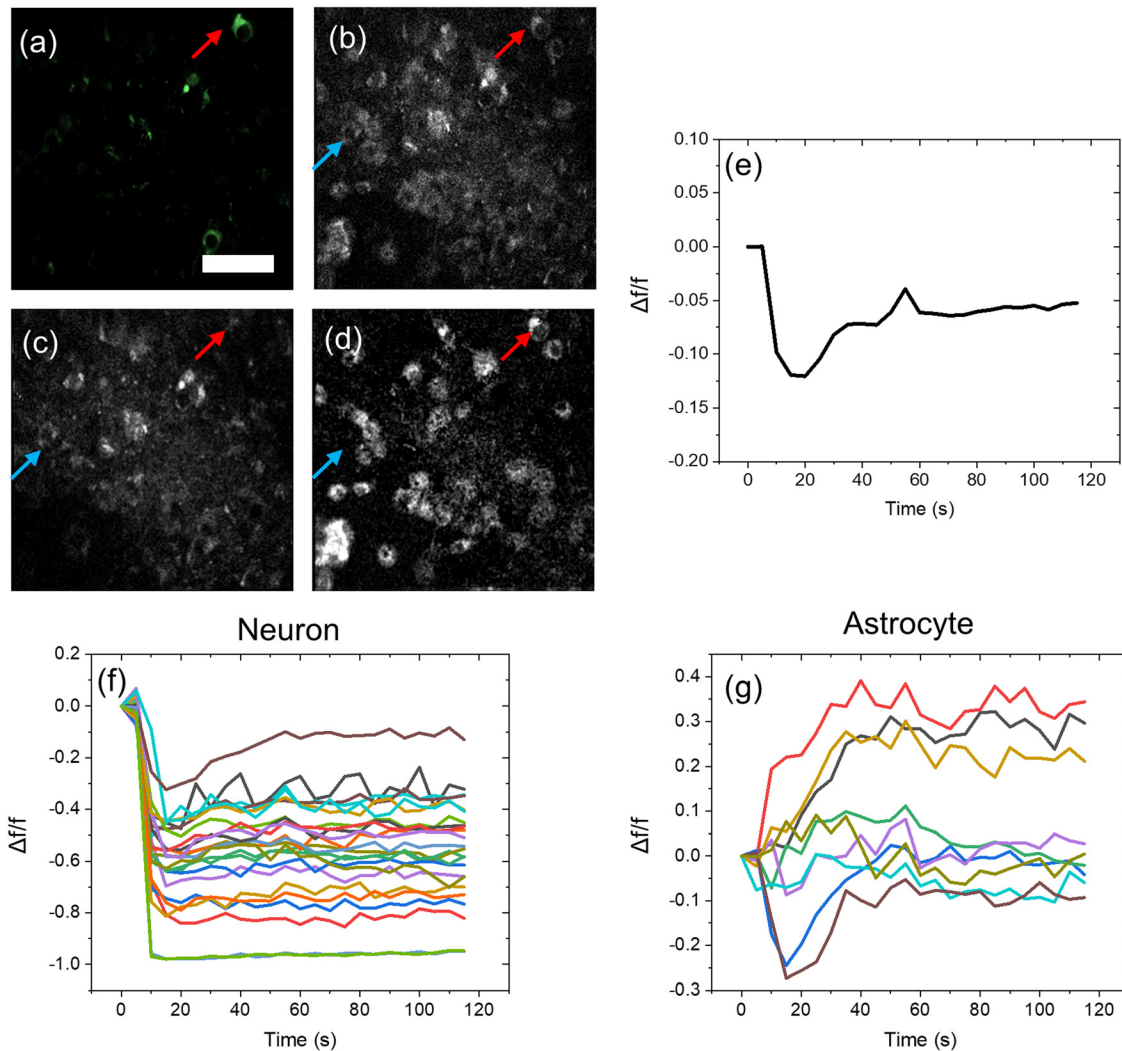


FIG. 2. 2PF NAD(P)H and GCaMP6s imaging of hippocampal cultures following 100 μ M glutamate stimulation. (a) GCaMP6s imaging of a region containing spontaneously firing neurons (red arrows) prior to stimulation. (b) and (c) NAD(P)H 2PF images (b) before and (c) 2 min after stimulation show a cellular dependence in the response leading to the sharp fluorescence decrease in some cells, compared to a slight fluorescence increase in others. (d) The image obtained by subtracting the image in (c) from the image in (b) shows that this sharp decrease exists in only a subpopulation of cells in the FOV. Red arrows correspond to an identified neuron, and blue arrows correspond to a cell identified as an astrocyte. (e) Longitudinal plot of NAD(P)H dynamics (measured by the change in fluorescence divided by the baseline fluorescence value) in response to stimulation across the entire FOV. (f) Longitudinal plot of the NAD(P)H response in individual neurons. (g) Longitudinal plot of the NAD(P)H response in individual astrocytes. The scale bar represents 50 μ m. In the associated video, the red arrow corresponds to an identified neuron and the blue arrow corresponds to a cell identified as an astrocyte. The red dot denotes the onset of neuronal activation. Multimedia view: <https://doi.org/10.1063/5.0031348.1>

and neurons upon stimulation. Results suggest that these cell types exhibit distinct metabolic dynamics upon stimulation, as has been previously suggested by the ANLS hypothesis.

Fluorescence lifetime imaging was also performed to further characterize these NAD(P)H transients (Fig. 3). The decreased SNR of the acquired datasets results in a few important trends that can be observed. Figures 3(a), 3(d), and 3(g) show images acquired before stimulation, within 10 s following stimulation, and 2 min post-stimulation, respectively. Fluorescence decay curves shown in Figs. 3(b), 3(c), 3(e), 3(f), and 3(h) were constructed through summation of fluorescence decay curves

over the 20×20 pixel areas denoted by the red and blue boxes, corresponding to a neuron and astrocyte, respectively, over the 5 s integration window of each FLIM image. In cells consistent with neurons [red boxes in Figs. 3(c) and 3(f)], a sharp increase in the NAD(P)H lifetime can be seen immediately following stimulation [Figs. 3(c), 3(f), and red curve in 3(i)], indicative of an increase in oxidative phosphorylation, as has been suggested previously.⁷ However, due to the sharp decrease in NAD(P)H fluorescence emission levels, lifetime analysis at later time points becomes difficult due to the low SNR of the decreased neuronal NAD(P)H signal [red curve in Fig. 3(i)]. Analysis of surrounding

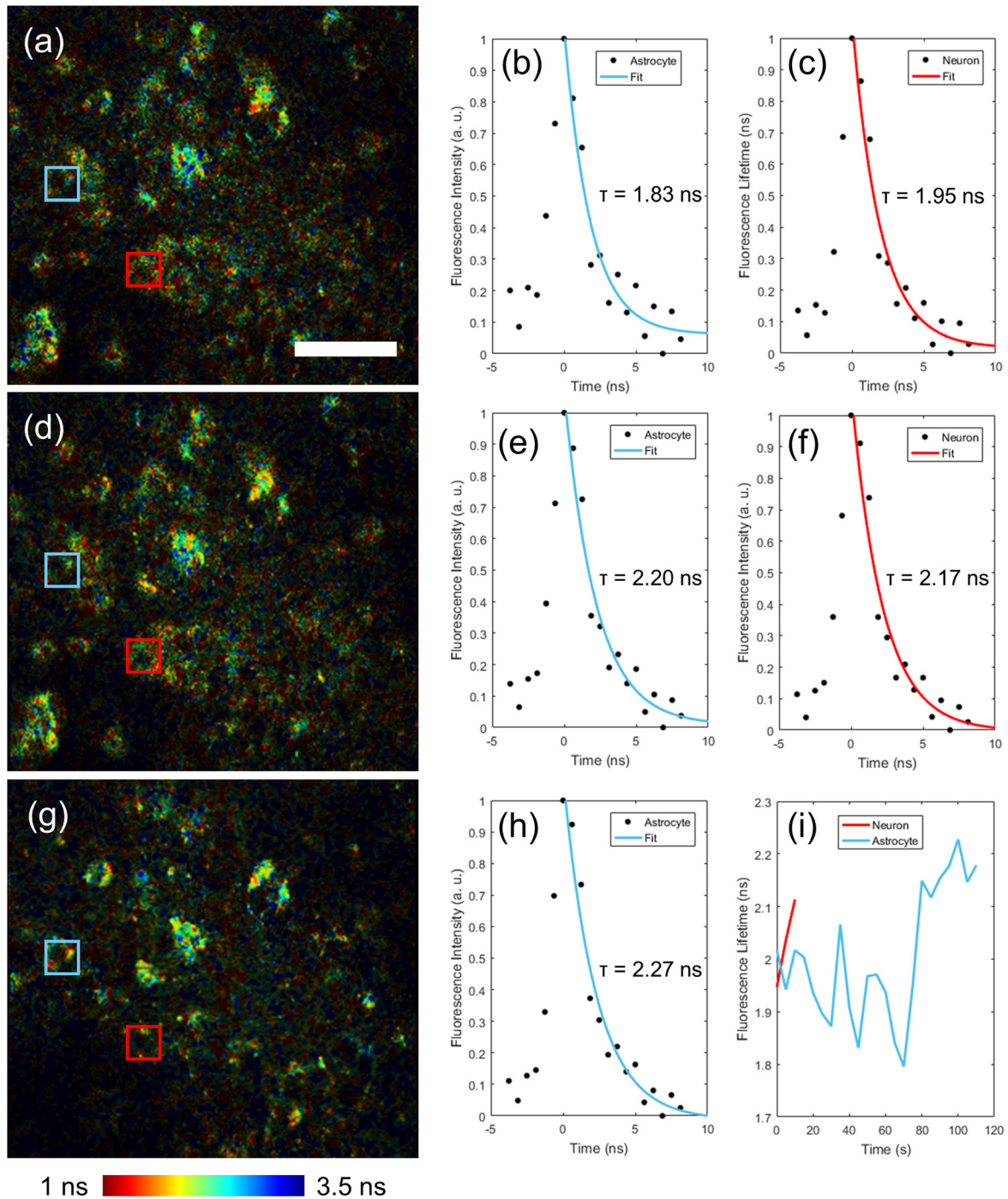


FIG. 3. 2P-FLIM NAD(P)H imaging of hippocampal neuron cultures following 100 μ M glutamate stimulation. Images acquired (a) before, (d) within 10 s following stimulation, and (g) 2 min following stimulation show lifetime dynamics in cells identified as astrocytes (blue boxes) and as neurons (red boxes). Fluorescence decay curves constructed through summation of the fluorescence decay signal over a 20×20 pixel ROI from the astrocyte (b), (e), and (h) and neuron (c) and (f) over the area of the blue and red boxes, respectively, over the 5 s temporal integration window of each FLIM image shows an increase in the lifetime in these cells after stimulation. (i) Plots of the lifetime dynamics in the cells corresponding to the red and blue boxes in (a), (d), and (g) corresponding to the average lifetime over the ROI. Due to the dynamic decrease in NAD(P)H fluorescence levels following neuronal activation, the NAD(P)H lifetime in these cells (red trace) cannot be accurately tracked past the initial “dip” phase. The scale bar represents 50 μ m.

astrocytes additionally revealed a noticeable increase in the fluorescence lifetime at later time points following stimulation [Figs. 3(b), 3(e), 3(h), and blue curve in 3(i)], suggesting an increase in oxidative phosphorylation at these later stages. It is important to note that in addition to binding to mitochondria, NADH is also capable of binding to lactate dehydrogenase (LDH), which has been observed through analysis of the bound NAD(P)H fluorescence lifetime (τ_2) without a significant change observed in the mean NAD(P)H lifetime (τ_m).²⁶ However, as the extracted NAD(P)H lifetime here is based on a single-exponential fit, it is unlikely to be sensitive to dynamics associated with NADH-LDH binding.

In order to assess these effects over a larger area, wide FOV 2PF GCaMP6s and 2P-FLIM NAD(P)H imaging was enabled by acquiring

a 10×10 mosaic of images over a field of approximately $2 \text{ mm} \times 2 \text{ mm}$ using a motorized translation stage. 2P-FLIM imaging was performed here with temporal integration of images over one second (20 individual frames acquired at 20 frames per second) at each stage position with no spatial binning or filtering applied. In a previous study, a similar mosaicing procedure was performed utilizing a traditional time-correlated single photon counting (TCSPC)-based 2P-FLIM system, which required approximately 3 h to acquire a 10×10 image mosaic.²⁷ Here, the full mosaic was acquired in approximately 2 min. 2PF GCaMP6s and 2P-FLIM NAD(P)H mosaics were acquired sequentially after tuning the excitation laser from 750 nm for NAD(P)H imaging to 920 nm for GCaMP6s imaging. Mosaics from the NAD(P)H and GCaMP6s channels were acquired before and after

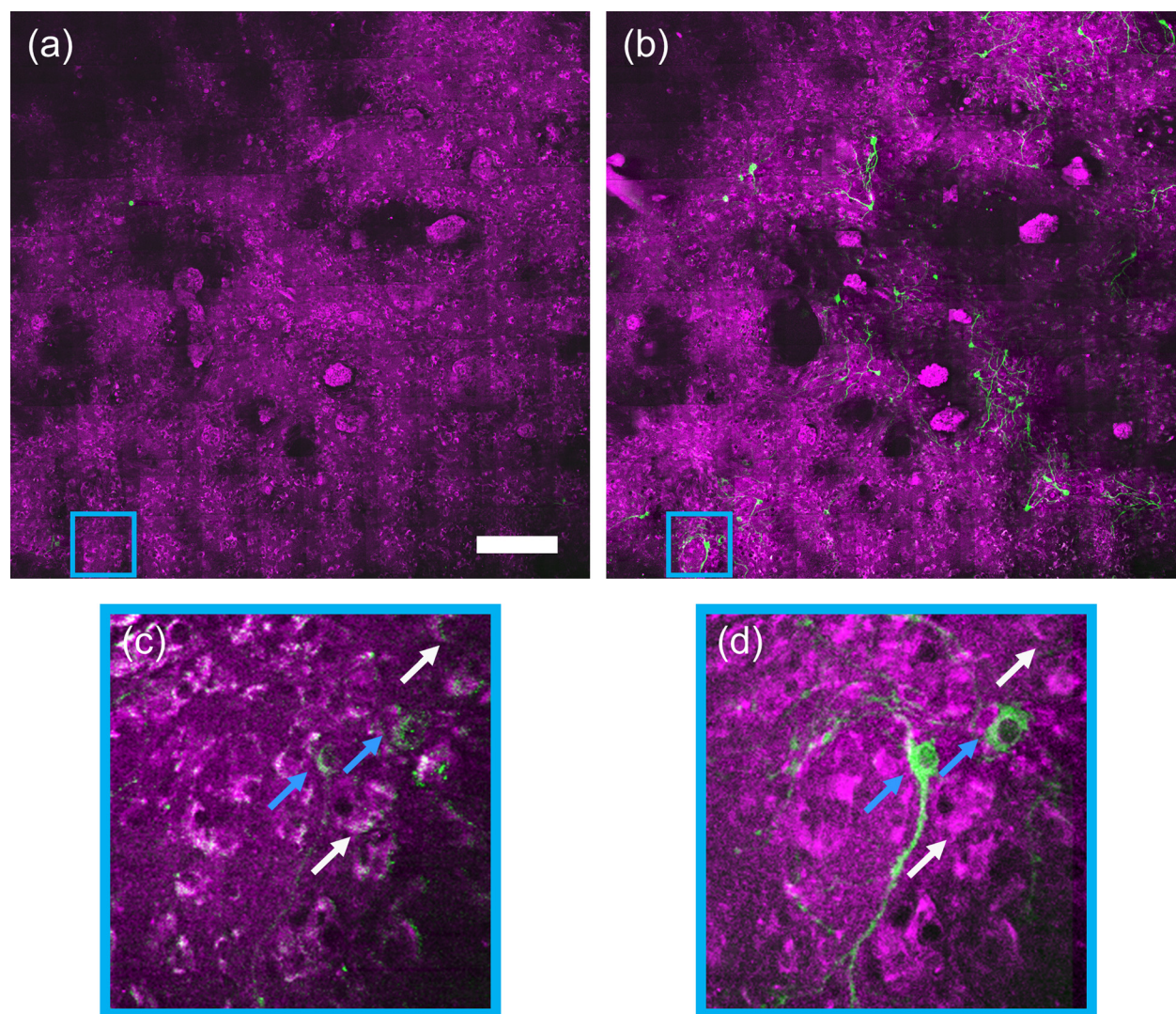


FIG. 4. Large FOV 2PF GCaMP6s and NAD(P)H imaging of neuronal activation and cellular metabolism. Overlaid 2PF imaging of NADH (magenta) and GCaMP6s (green) fluorescence images (a) before and (b) approximately 5 min following the application of $100 \mu\text{M}$ glutamate. (c) and (d) Zoomed regions corresponding to the blue boxes in (a) and (b), respectively. Following stimulation, an increase in neuronal activity can be observed in several regions corresponding to the enhanced fluorescence from GCaMP6s. Similarly, an increase in NAD(P)H fluorescence, mostly confined to astrocytes, can be clearly observed. The scale bar represents $200 \mu\text{m}$.

addition of glutamate to a final concentration of $100\ \mu\text{M}$ to assess the effects of neuronal activation across large cellular regions. Co-registered overlays of the 2PF NAD(P)H (magenta) and GCaMP6s (green) signals before [Fig. 4(a)] and approximately 5 min after [Fig. 4(b)] stimulation are shown in Fig. 4. Zoomed regions of these images (blue rectangles) in Figs. 4(c) and 4(d) show increased GCaMP6s fluorescence signals due to neuronal activation (blue arrows), which stand in contrast to the strong cellular NAD(P)H fluorescence likely from surrounding astrocytes (white arrows).

Corresponding 2P-FLIM images before and after stimulation are shown in Figs. 5(a) and 5(b), respectively. Figures 5(c) and 5(d) show zoomed regions highlighting interesting lifetime features, including the long NAD(P)H lifetime of an axon or dendrite (white arrows).

Nearby, the NAD(P)H fluorescence emission in neighboring cells appears to increase following stimulation and exhibit a decreased fluorescence lifetime, suggestive of glycolysis within surrounding cells. These results demonstrate the capability of our system to probe large areas of dynamic cellular activity, permitting assessment of neuronal activity and metabolism across large cell populations.

In practice, cellular-level optical imaging of the metabolic response to neuronal activation is challenging due to the high speed of neuronal dynamics, dense tissue structure, and decreased NAD(P)H fluorescence compared to many other tissues. While previous studies have relied on the use of low-resolution, wide-field imaging or high-resolution imaging with limited cellular contrast of neuronal NAD(P)H, the imaging system presented here is capable of

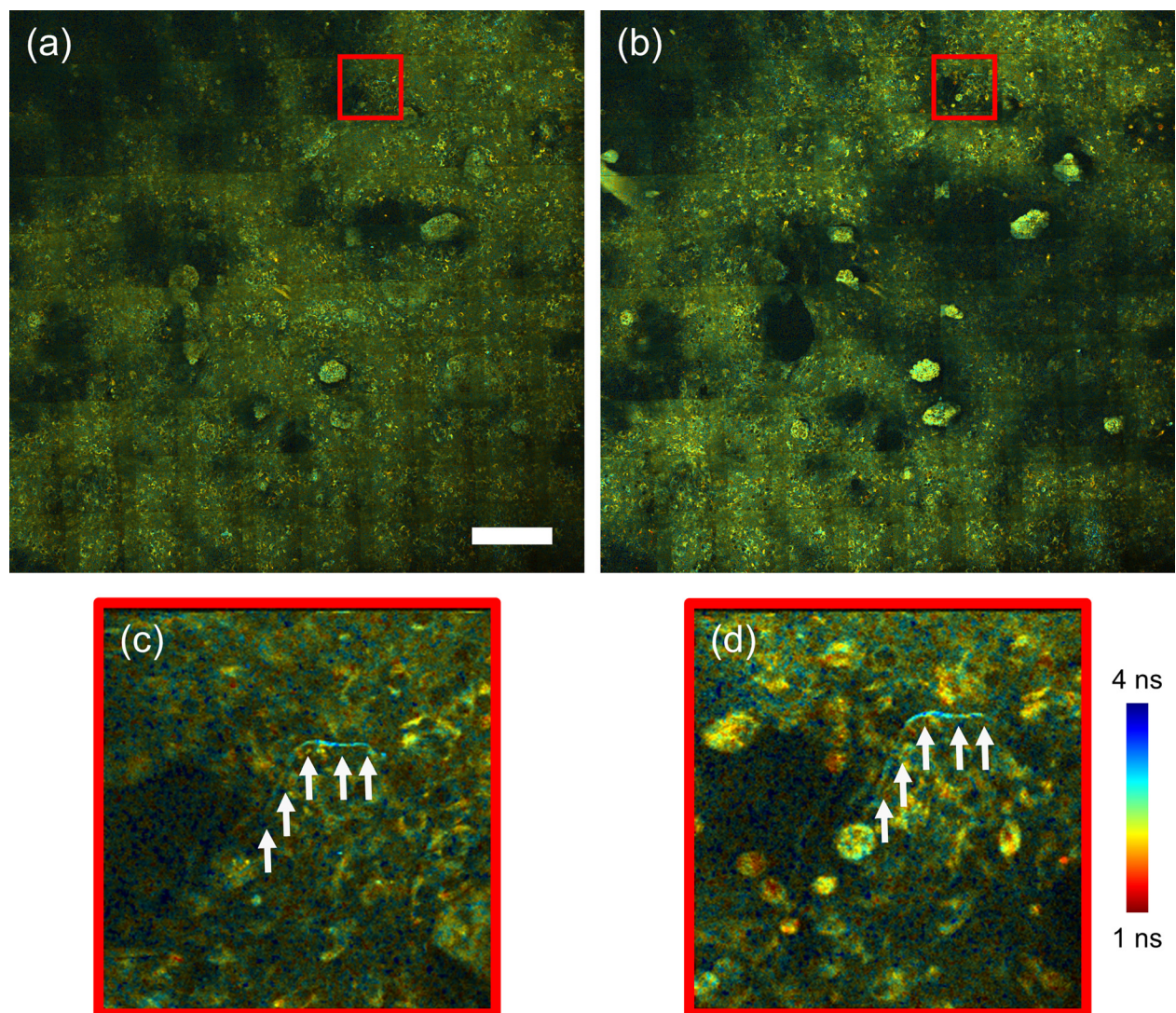


FIG. 5. Large FOV 2P-FLIM imaging of neuronal activation corresponding to the images shown in Fig. 4. (a) and (b) 2P-FLIM images of neuronal cultures (a) before and (b) approximately 5 min after stimulation. (c) and (d) zoomed regions corresponding to the red boxes in (a) and (b), respectively. White arrows indicate a long lifetime region observed in an axon or dendrite. The scale bar represents $200\ \mu\text{m}$.

performing dynamic imaging of neuronal cultures with high contrast and cellular-level resolution. The combination of GCaMP6s fluorescence and NAD(P)H autofluorescence permits the study of metabolism following neuronal activity at the cellular level, with imaging rates capable of capturing NAD(P)H transients occurring within seconds following stimulation. This imaging system was employed to directly identify distinct metabolic pathways between individual astrocytes and neurons upon neuronal activation. Extending this approach to the study of metabolic dynamics in neuronal circuits with targeted stimulation and to the study of metabolic dynamics in intact hippocampal tissue is of great importance in furthering the understanding of the complex metabolic machinery of neuronal activation.

We thank Darold Spillman for assistance with logistical and information technology support. A.J.B. was supported in part by a National Science Foundation Graduate Research Fellowship (No. DGE-1144245) and by the Beckman Graduate Student Fellowship. J.L. and C.R. were supported in part by an NIH T32 Tissue Microenvironment training Grant (No. T32 EB019944). This research was supported in part by grants from the National Science Foundation (No. CBET 18-41539), the Air Force Office of Scientific Research (No. FA9550-17-1-0387), and the National Institutes of Health (No. R01 EB023232 and R01 CA213149). Additional information can be found at <http://biophotonics.illinois.edu>.

DATA AVAILABILITY

The data that support the findings of this study are available from the corresponding author upon reasonable request and through a collaboration agreement.

REFERENCES

- ¹L. Sokoloff, *Handbook of Physiology*, edited by J. Field, H. W. Magoun, and V. E. Hall (American Physiological Society, Washington DC, 1960), Vol. 3, pp. 1843.
- ²P. T. Fox, M. E. Raichle, M. A. Mintun, and C. Dence, *Science* **241**, 462 (1988).
- ³P. Lipton, *Biochem. J.* **136**, 999 (1973).
- ⁴L. Pellerin and P. J. Magistretti, *Proc. Natl. Acad. Sci. U.S.A.* **91**, 10625 (1994).
- ⁵F. Boumezbeur, K. F. Petersen, G. W. Cline, G. F. Mason, K. L. Behar, G. I. Shulman, and D. L. Rothman, *J. Neurosci.* **30**, 13983 (2010).
- ⁶D. Smith, A. Pernet, W. A. Hallett, E. Bingham, P. K. Marsden, and S. A. Amiel, *J. Cereb. Blood Flow Metab.* **23**, 658 (2003).
- ⁷K. A. Kasischke, H. D. Vishwasrao, P. J. Fisher, W. R. Zipfel, and W. W. Webb, *Science* **305**, 99 (2004).
- ⁸P. J. Magistretti and L. Pellerin, *Cereb. Cortex* **6**, 50 (1996).
- ⁹C. M. Díaz-García, R. Mongeon, C. Lahmann, D. Koveal, H. Zucker, and G. Yellen, *Cell Metab.* **26**, 361 (2017).
- ¹⁰M. DiNuzzo, S. Mangia, B. Maraviglia, and F. Giove, *J. Cereb. Blood Flow Metab.* **30**, 586 (2010).
- ¹¹A. I. Ivanov, A. E. Malkov, T. Waseem, M. Mukhtarov, S. Buldakova, O. Gubkina, M. Zilberter, and Y. Zilberter, *J. Cereb. Blood Flow Metab.* **34**, 397 (2014).
- ¹²S. Mangia, I. A. Simpson, S. J. Vannucci, and A. Carruthers, *J. Neurochem.* **109**, 55 (2009).
- ¹³C. W. Shuttleworth, *Neurochem. Int.* **56**, 379 (2010).
- ¹⁴J. R. Lakowicz, H. Szmajnski, K. Nowaczyk, and M. L. Johnson, *Proc. Natl. Acad. Sci. U.S.A.* **89**, 1271 (1992).
- ¹⁵M. C. Skala, K. M. Riching, A. Gendron-Fitzpatrick, J. Eickhoff, K. W. Eliceiri, J. G. White, and N. Ramanujam, *Proc. Natl. Acad. Sci. U. S. A.* **104**, 19494 (2007).
- ¹⁶A. J. Walsh, R. S. Cook, H. C. Manning, D. J. Hicks, A. Lafontant, C. L. Arteaga, and M. C. Skala, *Cancer Res.* **73**, 6164 (2013).
- ¹⁷A. J. Bower, M. Marjanovic, Y. Zhao, J. Li, E. J. Chaney, and S. A. Boppart, *J. Biophotonics* **10**, 143 (2017).
- ¹⁸A. J. Bower, J. E. Sorrells, J. Li, M. Marjanovic, R. Barkalifa, and S. A. Boppart, *Biomed. Opt. Express* **10**, 6408 (2019).
- ¹⁹M. A. Yaseen, S. Sakadžić, W. Wu, W. Becker, K. A. Kasischke, and D. A. Boas, *Biomed. Opt. Express* **4**, 307 (2013).
- ²⁰Z. Liu, D. Pouli, C. A. Alonzo, A. Varone, S. Karaliota, K. P. Quinn, K. Münger, K. P. Karalis, and I. Georgakoudi, *Sci. Adv.* **4**, eaap9302 (2018).
- ²¹S. Kaech and G. Banker, *Nat. Protoc.* **1**, 2406 (2006).
- ²²A. J. Bower, J. Li, E. J. Chaney, M. Marjanovic, D. R. Spillman, and S. A. Boppart, *Optica* **5**, 1290 (2018).
- ²³T.-W. Chen, T. J. Wardill, Y. Sun, S. R. Pulver, S. L. Renninger, A. Baohan, E. R. Schreier, R. A. Kerr, M. B. Orger, V. Jayaraman, L. L. Looger, K. Svoboda, and D. S. Kim, *Nature* **499**, 295 (2013).
- ²⁴J. B. Pawley, *Handbook of Biological Confocal Microscopy* (Springer, 2006), p. 20.
- ²⁵A. E. Carpenter, T. R. Jones, M. R. Lamprecht, C. Clarke, I. H. Kang, O. Friman, D. A. Guertin, J. H. Chang, R. A. Lindquist, J. Moffat, P. Golland, and D. M. Sabatini, *Genome Biol.* **7**, R100 (2006).
- ²⁶J. T. Sharick, P. F. Favreau, A. A. Gillette, S. M. Sdao, M. J. Merrins, and M. C. Skala, *Sci. Rep.* **8**, 5456 (2018).
- ²⁷A. J. Bower, B. Chidester, J. Li, Y. Zhao, M. Marjanovic, E. J. Chaney, M. N. Do, and S. A. Boppart, *Quant. Imaging Med. Surg.* **7**, 24 (2017).